Materials Transactions, Vol. 45, No. 5 (2004) pp. 1700 to 1705

Mechanical Properties Related to Microstructural Variation of 6061 Al Alloy Joints by Friction Stir Welding

Won-Bae Lee[1,*1], Yun-Mo Yeon[2] and Seung-Boo Jung[1,*2]

[1]*Department of Advanced Materials Engineering, Sungkyunkwan University, 300 Cheoncheon-dong, Jangan-gu, Suwon, Kyounggi-do 440-746, Korea*
[2]*Department of Automated System, Suwon Science College, Hwasung, Kyounggi-do 445-742, Korea*

The microstructural change related with the mechanical properties of a friction stir welded 6061 Al alloy has been investigated under various welding conditions. Frictional heat and plastic flow during friction stir welding produced fine and equiaxed grains in the stir zone, macroscopically upset and elongated grains in the thermo-mechanically affected zone caused by dynamic recovery and recrystallization. The heat-affected zone, characterized by coarse precipitates, was formed beside the weld zone. Hardness distribution near the weld zone was strongly related to the behavior of precipitates and dislocation density. Especially, hardness of the SZ at a higher tool rotation speed was higher than that of a lower tool rotation speed due to higher density of spherical shaped re-precipitates. The joint strength was approximately 200 MPa which was lower than that of the base metal, 270 MPa, because softening region was formed around the weld zone.

(Received November 27, 2003; Accepted March 15, 2004)

Keywords: *friction stir welding, 6061 aluminum alloy, precipitate and dislocation behavior*

1. Introduction

Various Al alloys have specific properties and can be applied to many structural parts that need both light weight and high mechanical properties. However, when Al alloys are welded by a conventional fusion welding method to use as industrial frames or parts, various welding defects, such as voids, hot cracks and distortion which are related to the melting and solidification, would be formed in the weld zone. Moreover, the problems of fusion welded Al alloys which are related to the precipitation, dissolution and the loss of work hardening effect would occur near the weld zone.[1–4] Therefore, the solid state bonding technique is highly recommended to minimize many problems. Friction stir welding, invented by TWI in 1991, is a promising technique because it achieves superior joint quality of various of Al alloys.[1,5–8] Therefore, Al alloy frames joined by FSW have been used in the transportation industry such as the high speed rail way,[9] shipping[10] and external fuel tanks of rockets.[11]

Figure 1 shows a schematic illustration representing the friction stir welding process. Basically, in the FSW process, a nonconsumable tool with a specially designed rotating pin is entered into the abutting edges of sheets or plates to be welded. Once entered, the rotating tool produces frictional heat which makes the welded workpieces easily plastically deformed. The tool is then translated along the joint to complete the joining process.[12] Friction stir welding achieves solid phase joining by locally introducing frictional heat and plastic flow by the rotating welding tool with a resultant local microstructure change in Al alloys. The local microstructure determines the weld mechanical properties. Therefore, it is important to make clear the details of the microstructural evolution during the severe thermomechanical conditions imposed by FSW.

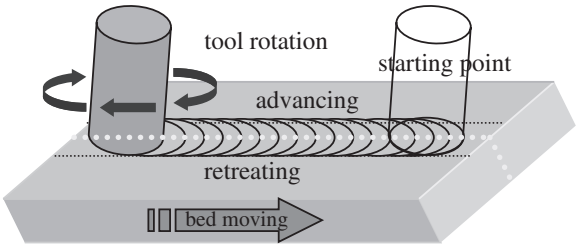

Fig. 1 Schematic illustrations of friction stir welding process and geometry of welded specimens.

Microstructural changes in the friction stir weld zone have been investigated for the various Al alloys in case of precipitation hardening Al alloys.[13–19] Results from these studies suggested that a dynamic recrystallization resulted in a fine grain equiaxed structure having a high angle grain boundaries occurred in the weld nugget or stir zone. The precipitation and dislocation behaviors in each region received a different thermomechanical condition were observed. The effects of friction stir welding parameters, especially the welding speed and tool rotation speed, on the microstructural change and mechanical properties of the friction stir welded Al alloys have not been well studied.

The objective of the present study is to observe the microstructural variation such as grain structure, behaviors of precipitation and dislocation and to evaluate mechanical properties of the friction stir welding of the 6061 Al alloy with different tool rotation and welding speeds.

2. Experimental Procedure

The material used was the 6061-T6 Al alloy with 140 mm in length, 70 mm in width and 4 mm in thickness. The chemical composition of the material is displayed in Table 1.

Friction stir welding has many welding parameters, such as the tool (including shoulder and screw-like probe) materials and design, tool rotation speed, welding speed and angle of

*1Graduate Student, Sungkyunkwan University
*2Corresponding author, E-mail: sbjung@skku.ac.kr

Table 1 Chemical composition of the 6061-T6 Al alloy (in mass%).

	Si	Fe	Cu	Mn	Mg	Cr	Zn	Ti	Al
6061	0.57	0.17	0.21	0.03	0.92	0.07	0.02	0.02	Bal

the tool. In this study, the tool rotation speed and welding speed were taken into account and changed from 131 rad/s (1250 rpm) to 377 rad/s (3600 rpm) and from 87 mm/min to 267 mm/min, respectively, because the generated heat in the weld zone strongly depends on both the tool rotation and welding speeds. The angle of the tool was fixed at 3 degrees to give sufficient stirring and compressive force to the weld zone. The welding tool was rotated in the clockwise direction and part, where welded plates were tightly fixed on the backing plate, was traveled.

Microstructural changes from the weld zone to the unaffected base material were examined using OM (Optical Microscopy) and TEM (Transmission Electron Microscopy). Specimens for observation of optical microstructures near the weld zone were prepared by the conventional polishing method followed by etching with the Keller agent. For TEM observation, thin-foil disk specimens with 3 mm in diameter were cut from various locations near the weld zone using an EDM (electron discharge machine) and were prepared by twinjet electro polishing in nitric acid/methanol solution at 243 K. This thin foils were observed at 300 kV using a JEOL transmission electron microscope. The composition of the precipitates was analyzed by the TEM-EDS (Energy Dispersive Spectroscopy) analysis system.

The Vickers hardness profile of the weld zone was measured on a cross section and perpendicular to the welding direction with a 100 gf load for 10 s. The tensile test was carried out at room temperature using an Instron-type testing machine with a cross head speed of 1.67×10^{-2} mm/s. To determine the tensile strength of the joint, tensile test specimens were sectioned in the transverse direction to the weld line by an EDM.

3. Results and Discussion

The top and bottom surfaces of the weld zone were very smooth and surface defects were not detected on both surfaces under wide range of the applied welding conditions.

Figure 2 shows an optical macrostructure and related microstructures of each region indicated in the macrostructure. The weld zone shows specific features compared with those of the fusion welded joints. SZ (stir zone, region d) represents a wider near the upper surface than lower surface like a semi-sphere shape because the upper surface experienced extreme deformation and frictional heat caused by directly contacting welded plates with a cylindrical tool shoulder. Local variation of the microstructure was produced because each weld zone received a different thermomechanical condition.[16)]

Macroscopic examination of the weld zone reveals a relative non-symmetric SZ which was mainly associated with the tilt angle of the tool and the relation between the tool rotation direction and welding direction.[20)] It is apparent that the weld zone exhibits a high degree of continuity and no

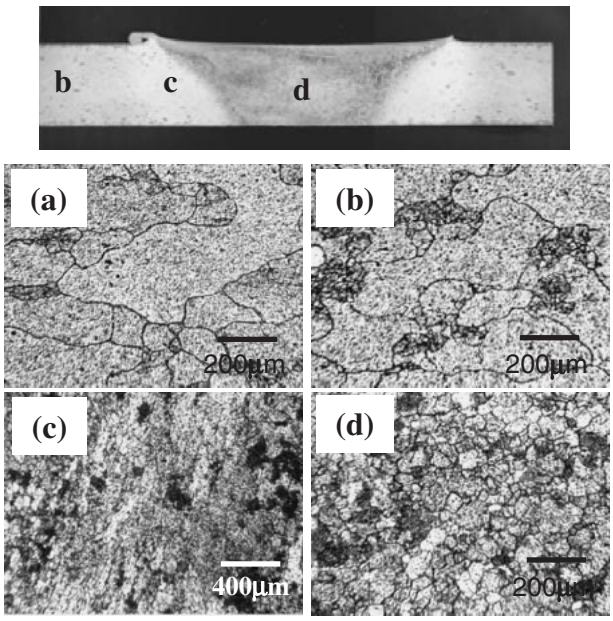

Fig. 2 Cross-sectional macrostructures of the weld zone and related microstructures indicated in the macrograph: (a) BM (base metal), (b) HAZ (heat affected zone), (c) TMAZ (thermo-mechanically affected zone), (d) SZ (stir zone).

porosity.

Unlike that of the base metal (BM, a), SZ (d) has fine and equiaxed grains and the grain size is much smaller than that of the BM. This structure was produced by the dynamic recrystallization and static grain growth after welding,[21,22)] which was caused by the frictional heat and plastic deformation. It is evident that the original grain structure was microscopically upset in the thermo-mechanically affected zone (TMAZ, c) and the transient microstructure between SZ and heat affected zone (HAZ, b) was obtained. The elongated and dynamic recovered grain structure[15)] is characterized in TMAZ because the thermal and deformation condition was not sufficient to produce the recrystallized grain structure.

The HAZ has a similar grain size with the unaffected BM. The mechanical and temperature conditions in the HAZ were not sufficient to promote grain growth or macroscopically to deform the BM.

The transverse macroscopic changes of the FSWelded 6061 Al alloy with each welding conditions are shown in Fig. 3. The area of the weld zone decreases with increasing the welding speed and decreasing the tool rotation speed. From the results of simulated and experimental methods regarding temperature distribution in the weld zone with welding parameters,[23,24)] a higher tool rotating and lower welding speed resulted in a higher temperature and slower cooling rate in the weld zone after welding. The welded plate was more easily plasticized and a wider range of the weld zone was mechanically affected in the present welding conditions.

The weld zone defects may be formed by the estimated two conditions. One is the lack of stirring. The other is formed by the excessive release of stirred materials to the upper surface, which resultantly left voids in the weld zone. The former was

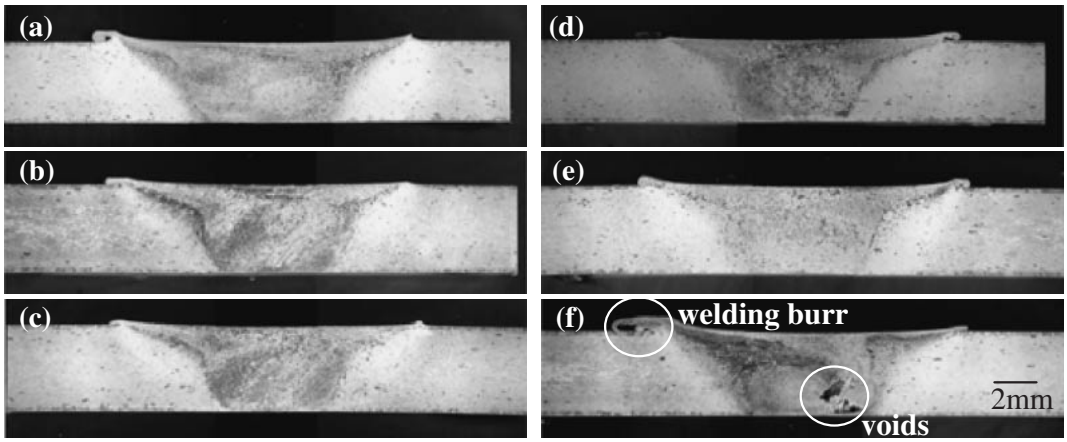

Fig. 3 Macrostructural variation with various welding conditions: (a) 87 mm/min, (b) 267 mm/min, (c) 342 mm/min: constant tool rotation speed 168 rad/s, (d) 131 rad/s, (e) 188 rad/s, (f) 377 rad/s: constant welding speed 267 mm/min.

observed in case of a lower heat input condition such as a lower rotation and higher welding speed. The latter was dominant under condition of a higher heat input condition such as a higher tool rotation and lower welding speed. As shown in Fig. 3(f), there exist some voids in the weld zone when the tool rotation speed was 377 rad/s at 267 mm/min welding speed because the stirred materials were excessively released from the SZ to upper surface of the weld zone. A large amount of welding burr on upper surface confirms the latter estimation as shown in Fig. 3(f). However, with exception of 377 rad/s of tool rotation speed, no weld defect was formed in the weld zone.

Some previous studies[15,21,22] have suggested that dynamically recrystallized grains were formed in the SZ during the stirring of FSW and then statically grew after passing of the welding tool. Therefore, the size of dynamically recrystallized grains may be affected by the welding condition. Figure 4 shows the grain size variation of the SZ with various welding conditions. As a whole, the grain size in the SZ increases with increasing tool rotation speed and decreasing welding speed. The grain size shows about 22 μm at the condition of 131 rad/s, 267 mm/min, and 40 μm at the condition of 377 rad/s, 267 mm/min. The grain size in the SZ with welding condition is consistent with the estimated temperature variation.

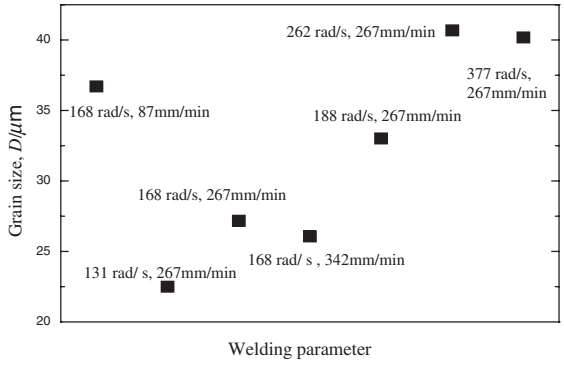

Fig. 4 Grain size distribution of the stir zone with various welding conditions.

Figure 5 represents the horizontal hardness profile near the weld zone along the centerline and TEM microstructures of SZ, HAZ (10 mm from the weld center) and BM. The weld zone exhibits a considerable softened region compared with the unaffected BM, which has a scattered hardness with a range of 90–95 HV. The total softened range is 18 mm and the region located 5–6 mm away from the weld center represents the minimum hardness. The hardness of SZ (c) and HAZ (b) are 75 HV and 77 HV, respectively. The minimum hardness beside SZ (5–6m from the weld center) can be explained by the coarsened precipitates and dynamic recovery grain structure.[15,25] The hardness distribution of each region (BM, HAZ, TMAZ, SZ) is not dependent on the grain size distribution with the reformulated Hall-Petch equation ($HV = 3\sigma_y$, $HV = H_0 + K_h D^{-1/2}$).[25]

In order to examine the effect of the microstructural variation on the hardness profile, the microstructures of each region: (a) BM, (b) HAZ (approximately 10 mm away from the weld center) and (c) SZ were observed by TEM.

The precipitation sequence of the pseudo-binary Al-Mg_2Si alloys is as follows: supersaturated solid solution $\rightarrow$ a needle-shaped precipitate (β'') $\rightarrow$ a rod-shaped precipitate (β') $\rightarrow$ a equilibrium β-Mg_2Si.[26–28] It is known that the needle-shaped precipitates of the coherent β'' phase contribute predominantly to the strength of the 6XXX series Al alloys.[29]

Precipitates existing in the BM (a) are composed of mainly Mg_2Si and some AlFeSi phases analyzed by EDS. The BM includes higher density of fine needle-shaped precipitates (or GPzone) and rarely distributed rod-shaped precipitates. However, fine needle-shaped precipitates were grown to be coarsened rod-shaped precipitates in the HAZ (b) by the frictional heat. A higher density of coarsened rod-shaped precipitates and lower density of fine precipitate can contribute to explain a lower hardness in the HAZ than that of the BM. SADPs (Selected Area Diffraction Pattern) acquired Al matrix and precipitates represents a similar crystallographic structure. The Mg_2Si phase has a similar crystal structure (FCC) with that of Al matrix. Both BM and HAZ represent relatively lower density of dislocations.

SZ (c) is characterized by higher density of dislocations in

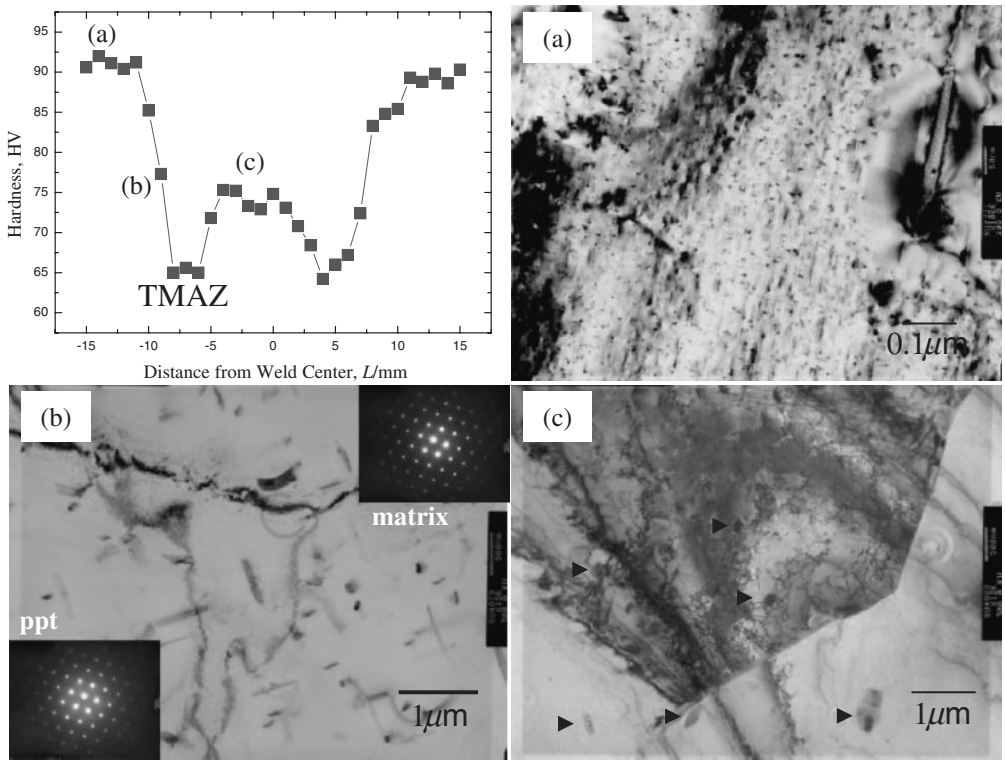

Fig. 5 Hardness distribution near the weld zone with the conditions of 168 rad/s, 267 mm/min and TEM microstructures of each region: (a) BM, (b) HAZ, (c) SZ. (▶: re-precipitates)

grains, dissolution of precipitates in the BM and re-precipitates. A higher density of dislocations with network structure observed in the recrystallized grains of the SZ implies that plastic deformation may have been introduced by FSW and recrystallized grains were produced by the dynamic process. Precipitates in the BM appeared to be dissolved into the Al matrix and re-precipitated in the SZ during the cooling stage because SZ experienced a higher temperature and slow cooling rate. Re-precipitates are mainly observed on the dislocation pile-up or subgrain boundary, providing evidence that dislocations were the preferential site for nucleation and growth of precipitate on cooling during welding thermal cycle. However, re-precipitates have a different morphology like spherical-shaped and extraordinary lager than needle-shaped precipitates existed in the BM. Su *et al.* explained this reason as the different precipitation mechanism between the SZ and BM. In the SZ, which experienced the dynamic recryatllization, the nucleation process changes from homogeneous to heterogeneous, with precipitate nucleating heterogeneously at dislocation.[15] The observation of high density of dislocation in SZ demonstrates that dislocations were favorable nucleation site for these precipitates. Precipitation on the dislocation appears to be directly related to the equilibrium phase and the growth of precipitates on the dislocation appears faster than in the bulk with a lower density of dislocation.

Though density of precipitates remarkably decreased in the SZ due to the dissolution in the Al matrix, the hardness is higher than that of region located 5–6 mm away from the weld center. The reasons why the SZ has a higher hardness are explained by a higher density of the dislocation network structure and spherical shaped re-precipitates because distributed precipitates pinned a dislocation movement. SZ also included fine grains with a tendency to high angle grain boundaries[13–18] which acted as the obstacle of dislocation movement.

Figure 6 shows the hardness distribution of the SZ with tool rotation speeds. There was no variation of hardness distribution near the weld zone according to welding speed which was applied in this study. This was similar result to that of M. Ericsson *et al.*[30] However, the hardness of the SZ increases with the tool rotation speed. The TEM micrographs (Fig. 7) reveal that larger amount of spherical shape

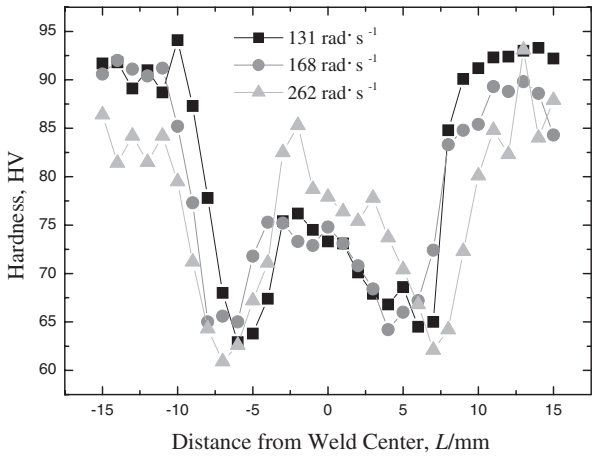

Fig. 6 Hardness distribution near the weld zone with various tool rotation speeds.

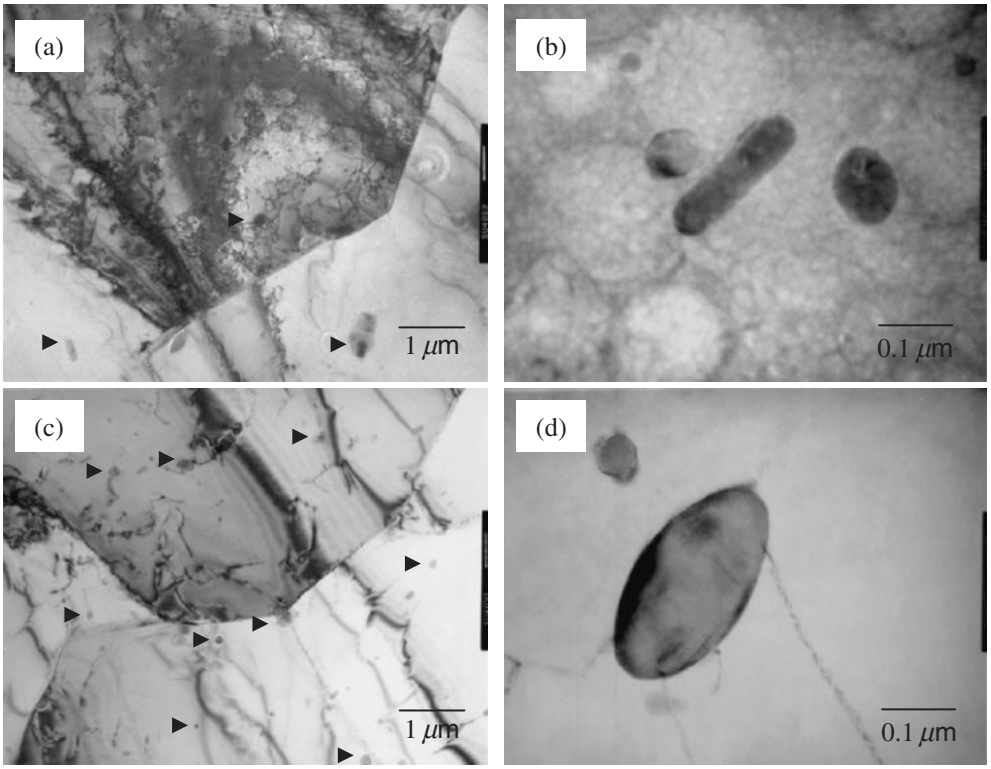

Fig. 7 TEM microstructures of the stir zone: (a) and (b) 168 rad/s, (c) and (d) 262 rad/s. (▶: re-precipitates)

precipitates are observed in the SZ of 262 rad/s tool rotation speed. Helical dislocation loops and dislocations pinned by particles are also observed. A higher tool rotation speed resulted in the lower cooling rate because SZ reached a higher temperature. Therefore, a slower cooling sufficiently promoted the re-precipitation of dissolved precipitates. Though the SZ in case of a higher tool rotation speed is characterized by lager grains and lower density of dislocations, higher density of spherical shape precipitates can contribute to a higher hardness than that of a lower tool rotation speed in the SZ.

Figure 8 shows the relation between grain size and hardness value near the weld zone with welding conditions.

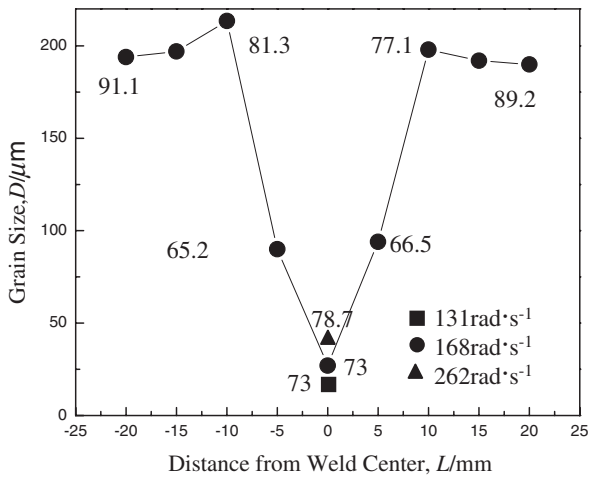

Fig. 8 Grain size distribution near the weld zone with welding conditions. (Numerals represent the hardness value)

From above mentioned the reformulated Hall-Petch equation, the hardness in general metallic materials is proportional to the $D^{-1/2}$ (D: grain size). However, hardness distribution near the FSWed 6061 Al alloy wasn't satisfied with this equation because the hardness profile strongly depended on the precipitate distribution and dislocation density rather than the grain size.

Figure 9 shows the UTS (ultimate tensile strength), YS (yield strength) and elongation with various welding conditions. UTS, YS and elongation of the 6061 Al BM were experimentally measured and represents 270 MPa, 150 MPa and 15%, respectively. Except for the condition of 377 rad/s of tool rotation speed (including large void in the SZ), UTS, YS and elongation of the joints are approximately 200 MPa, 80 MPa and 10%. The joints properties show slightly lower values than those of the BM because tensile specimens were fractured around minimum hardness region (5–6 mm away from the weld center) regardless of welding conditions except for 377 rad/s of tool rotation speed. The tensile properties acquired from the transverse tensile test were not significantly affected by the welding condition without defects.

4. Conclusions

The present work examined the microstructure and mechanical properties of the FSWelded 6061 Al alloy under various welding conditions. The results of this work were as follows:

(1) The weld zone was divided into three regions by using OM: (1) SZ had fine and equiaxed grains, (2) TMAZ had a severely upset and elongated grain structure and existed

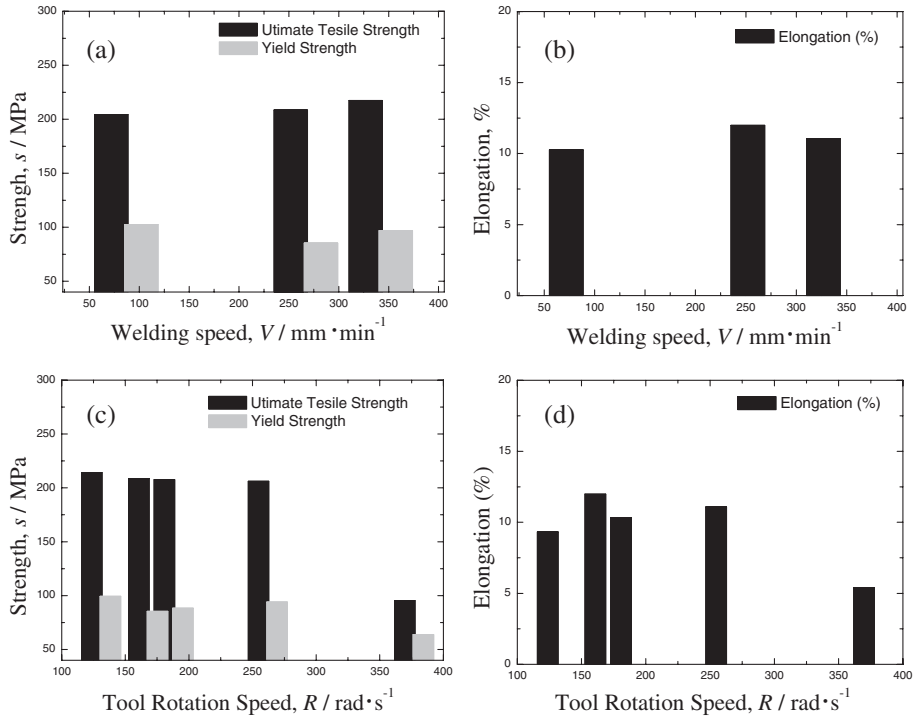

Fig. 9 UTS, YS and elongation variation with welding condition: (a) UTS and YS, (b) elongation: welding speed variable, (c) UTS and YS, (d) elongation: tool rotation speed variable.

between SZ and HAZ, (3) HAZ was no difference in grain size compared with that of the BM.

(2) A wide range of welding condition could be applied to join the 6061 Al alloy by friction stir welding except for the excessive tool rotation speed of 377 rad/s.

(3) The friction stir welded zone of the 6061 Al alloy represented a specific local variation of precipitates, dislocation and grain structures under different thermo-mechanical conditions. SZ characterized by dynamic recrystallization had a higher density of dislocation network structure and spherical shaped re-precipitates. HAZ was characterized by coarsened precipitates.

(4) The hardness distribution near the weld zone was mainly dependent on the behavior of precipitates and dislocation density rather than grain size. Especially, in the case of a higher tool rotation speed with lager grin size, hardness of the SZ represented a higher value than that of the lower tool rotation speed because the density of spherical shape re-precipitates increased.

(5) Joints properties of the 6061 Al alloy by FSW showed a lower value than those of the BM because the softening region were produced.

REFERENCES

1) M. B. Ellis and M. Strangwood: Mater. Sci. Tech. **12** (1996) 970–977.
2) L. A. Guitterez, G. Neye and E. Zschech: Weld. J. **75** (1996) 115s–121s.
3) J. Hagstron and R. Sandstrom: Sci. Technol. Weld. Join. **2** (1997) 199–208.
4) A. J. Sunwoo and J. W. Morris Jr: Weld. J. **68** (1989) 262s–268s.
5) C. J. Dawes and W. M. Thomas: Weld. J. **75** (1996) 41–45.
6) W. M. Thomas and E. D. Nicholas: Mater. Des. **18** (1997) 269–273.
7) W. B. Lee, Y. M. Yeon and S. B. Jung: Mater. Sci. Eng. A **355** (2003) 154–159.
8) W. B. Lee, Y. M. Yeon and S. B. Jung: Scripta Mater. **49** (2003) 423–428.
9) H. Okamura, K. Aoba and M. Ezumi: J. Jpn. Inst. Light Met. **50** (200) 166–171.
10) S. Kallee, D. Richardson and I. Henderson: Schweissen Schneiden (Welding cutting) **49** (1997) 904–909.
11) M. R. Johnsen: Weld. J. **78** (1999) 35–39.
12) C. J. Dawes and W. M. Thomas: TWI Bulletin **6** (1995) 138–141.
13) C. G. Rhode, M. W. Mahoney, W. H. Bingel, R. A. Spurling and C. C. Bampton: Scripta Mater. **36** (1997) 69–75.
14) M. W. Mahoney, C. G. Rhodes, J. G. Flintoff, R. A. Spurling and W. H. Bingel: Metall. Mater. Trans. A **29** (1998) 1955–1964.
15) J.-Q. Su, T. W. Nelson, R. Mishra and M. Mahoney: Acta Mater. **51** (2003) 713–729.
16) G. Liu, L. E. Murr, C.-S. Niou, J. C. McClure and F. R. Vega: Scripta Mater. **37** (1997) 355–361.
17) L. E. Murr, G. Liu and J. C. McClure: J. Mater. Sci. **33** (1998) 1243–1251.
18) Y. S. Sato, H. Kokawa, M. Enomoto and S. Jorgan: Metall. Mater. Trans. A **30** (1999) 2429–2437.
19) Y. S. Sato, H. Kokawa, M. Enomoto, S. Jorgan and T. Hashimoto: Metall. Mater. Trans. A **30** (1999) 3125–3130.
20) W. M. Thomas and E. D. Nicholas: Mater. Design **18** (1997) 269–273.
21) Y. S. Sato, H. Kokawa, K. ikeda, M. Enomoto, S. Jorgan and T. Hashimoto: Metall. Mater. Trans. A **32** (2001) 941–948.
22) K. V. Jata and S. L. Semiatin: Scripta Mater. **43** (2001) 743–749.
23) C. M. Chen, R. Kovacevic: Int. J. Mach. Tool Manu. **43** (2003) 1319–1326.
24) P. Ulysse: Int. J. Mach. Tool Manu. **42** (2002) 1549–1557.
25) Y. S. Sato, M. Urata, H. Kokawa and K. Ikeda: Mater. Sci. Eng. A **354** (2003) 298–305.
26) H. W. L. Philips: J. Inst. Met. **72** (1946) 151.
27) M. H. Jacobs: Philos. Mag. **26** (1972) 1–13.
28) H. Westehgen and N. Ryun: Z. Metallkd. **70** (1997) 528–35.
29) D. L. Zhang and L. Zheng: Metall. Mater. Trans. A **27** (1996) 3983–3991.
30) M. Ericsson and R. Sandstrom: Int. J. Fatigue **25** (2003) 1379–1387.